

**The following resources related to this article are available online at [www.sciencemag.org](http://www.sciencemag.org) (this information is current as of December 11, 2009):**

**Updated information and services**, including high-resolution figures, can be found in the online version of this article at:

<http://www.sciencemag.org/cgi/content/full/322/5909/1816>

**Supporting Online Material** can be found at:

<http://www.sciencemag.org/cgi/content/full/322/5909/1816/DC1>

This article has been **cited by** 2 article(s) on the ISI Web of Science.

This article appears in the following **subject collections**:

Materials Science

[http://www.sciencemag.org/cgi/collection/mat\\_sci](http://www.sciencemag.org/cgi/collection/mat_sci)

Information about obtaining **reprints** of this article or about obtaining **permission to reproduce this article** in whole or in part can be found at:

<http://www.sciencemag.org/about/permissions.dtl>

# Matching Glass-Forming Ability with the Density of the Amorphous Phase

Y. Li,<sup>1,2\*</sup> Q. Guo,<sup>1,2</sup> J. A. Kalb,<sup>1,3†</sup> C. V. Thompson<sup>1,3\*</sup>

The density of the amorphous phase of metals is generally thought to be related to glass formation, but this correlation has not been demonstrated experimentally to date. In this work, systematic deflection measurements using microcantilevers and a combinatorial deposition method show a correlation between glass-forming ability and the density change upon crystallization over a broad compositional range in the copper-zirconium binary system. Distinct peaks in the density of the amorphous phase were found to correlate with specific maxima in the critical thickness for glass formation. Our findings provide quantitative data for the development of structural models of liquids that are readily quenched to the amorphous state. The experimental method developed in this work can facilitate the search for new glass-forming alloys.

**M**etallic glasses are amorphous metals that do not have a structure with long-range atomic order like crystalline materials do, but have pronounced short- and medium-range order at the atomic scale. Because of their very different properties as compared to those of their crystalline counterparts, metallic glasses are very promising materials for future structural, chemical, and magnetic applications (1, 2). The packing density of the amorphous phase is a key consideration in studying the formation of metallic glasses (2–5). A liquid of high packing density (6–8) has a low free volume content and a correspondingly low atomic mobility (9–11). Upon quenching, such a liquid is expected to have a strong kinetic constraint on nucleation and the subsequent growth of crystals. This has been the basis for recent theoretical studies (12, 13) of structural models of metallic glasses, in which a correlation between compositions having especially dense packing and compositions that are known to quench to the glassy state at relatively low cooling rates was sought, but not obtained. Earlier studies of the density of glasses, based on the Archimedes method, have been mostly limited to relatively narrow compositional ranges of ternary and quaternary alloys with large critical sample sizes for glass formation (14–16), and no correlation between density and the ease of glass formation has been demonstrated.

We have developed a method for the measurement of density changes, using microfabricated Si-rich silicon nitride (SiN) cantilevers (17). Owing to the small size and close spacing of the cantilevers, the deposition of alloy films with compositions that varied in a controlled way from cantilever to cantilever allowed a combinatorial approach to measurements of density changes for a broad range of compositions, with high compositional resolution. This process is schematically illustrated in fig. S1. Heating-induced crystallization of the initially amorphous Cu-Zr films causes an increase in density (a decrease in volume) that causes an upward deflection of the cantilevers, as a result of the tensile elastic mismatch strain developed at the interface between the film and the cantilever. By measuring the magnitude of the cantilever tip deflection after crystallization, the corresponding density change in the film can be determined as a function of composition. Results obtained in this way were compared with the critical thicknesses for glass formation determined with the wedge-casting technique (fig. S3). The effective cooling rate in these wedge-casting experiments

is uniform for all compositions tested, and the critical thickness for glass formation can serve as a consistent measure of glass-forming ability. A binary alloy system is particularly suitable for this study because of the relatively simple variation in composition. The Cu-Zr system was selected, in which glass formation has been extensively studied, particularly in the compositional range of the current study, from  $\text{Cu}_{47}\text{Zr}_{53}$  to  $\text{Cu}_{68}\text{Zr}_{32}$  (18–21).

Freestanding, low-stress, SiN microcantilevers  $216 \pm 3$  nm thick were fabricated with standard microfabrication techniques (17). Cu-Zr films with thicknesses of  $128 \pm 4$  nm were sputter-deposited on the cantilevers by means of separate elemental sources. The deposition ranges of the two sources overlapped, but the two deposition fluxes varied over the surface of the wafer, so that the composition of the films deposited on a row of cantilevers varied monotonically from Zr-rich to Cu-rich [a schematic illustration of the experimental configuration can be found in the supporting online material (SOM)]. To avoid oxidation of the film during annealing, a thin ( $15 \pm 5$  nm) Pt capping layer was sputter-deposited on top of all the cantilevers. The final structure of the cantilever is schematically shown in Fig. 1. The film composition was determined by energy-dispersive x-ray spectroscopy (EDX), with an error estimated to be within 1.0 atomic %. X-ray diffraction (XRD) analysis was carried out at different locations along the row of cantilevers, and the as-deposited structure of the film was confirmed to be fully amorphous everywhere. Samples were then annealed in a furnace at  $600^\circ\text{C}$  for 5 min, in a vacuum of  $5 \times 10^{-5}$  torr. This led to complete crystallization of the Cu-Zr films (22), as determined by post-annealing XRD analysis. The upward deflections of the microcantilevers were measured by correlating the focus conditions with measurements of the z-axis displacement of the objective lens in an optical microscope.

The as-fabricated stress-free SiN cantilevers had near-zero curvature. After deposition of the amorphous Cu-Zr films, the cantilevers curved downward (Fig. 2A), indicating that the as-deposited films were subject to a compressive

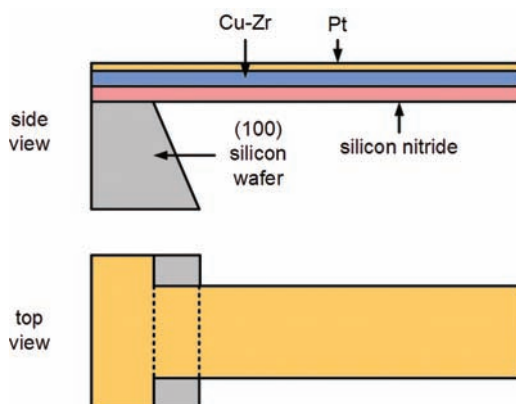


**Fig. 1.** Layer structure of a microcantilever with a fixed support (side view). A thin film of amorphous Cu-Zr (thickness  $128 \pm 4$  nm) was deposited on the SiN (thickness  $216 \pm 3$  nm). A thin Pt capping layer (thickness  $15 \pm 5$  nm) was used to prevent oxidation of the Cu-Zr film during annealing. The thicknesses of the layers are not drawn to scale.

<sup>1</sup>Singapore–Massachusetts Institute of Technology (MIT) Alliance, 4 Engineering Drive 3, Singapore 117576. <sup>2</sup>Department of Materials Science and Engineering, National University of Singapore, 7 Engineering Drive 1, Singapore 117576. <sup>3</sup>Department of Materials Science and Engineering, MIT, Cambridge, MA 02139, USA.

†Present address: Intel Corporation, Santa Clara, CA 95054, USA.

\*To whom correspondence should be addressed. E-mail: mseliy@nus.edu.sg (Y.L.); cthomp@mit.edu (C.V.T.)

residual deposition stress. Observation of residual compressive stress is not uncommon for vapor-deposited amorphous films (23, 24). When these samples are heated, the residual stress will be relaxed before crystallization occurs. This relaxation will result in a return to the original (near-zero) curvature of the cantilevers. Upon crystallization, the cantilevers deflect upward (Fig. 2B) with uniform radius of curvature  $r$ , resulting in a vertical tip deflection  $\delta$ , as shown in Fig. 2C. By measuring  $\delta$ , the density change upon crystallization  $(\rho_c - \rho_a)/\rho_a (>0)$  can be calculated, where  $\rho_a$  and  $\rho_c$  are the densities of the amorphous and crystalline phases, respectively. Details of this calculation can be found in (17) and the SOM (section 3), which includes fig. S2, which defines other important geometric characteristics of the bent beam.

For wedge-casting experiments, Cu-Zr alloys in the same composition range were prepared by arc-melting pure Zr (99.98%) and Cu (99.999%) and casting them in wedge-shaped molds. The critical thickness for glass formation was measured for each composition by optical microscopy of the wedge cross-sections. The critical thickness corresponds to the minimum cooling rate at which a glass will form, and is used as a measure of the ease of glass formation.

Figure 3A shows  $(\rho_c - \rho_a)/\rho_a$ . There are three local minima:  $2.64 \pm 0.02\%$  at  $\text{Cu}_{50.6}\text{Zr}_{49.4}$ ,  $2.88 \pm 0.02\%$  at  $\text{Cu}_{56.6}\text{Zr}_{43.4}$ , and  $2.52 \pm 0.02\%$  at  $\text{Cu}_{63.1}\text{Zr}_{36.9}$ . The overall range for the density change is 2.5 to 4.5%, which is typical for binary metallic glasses (3, 25). The measured changes in deflection are related to several phenomena

which include, but are not limited to, crystallization alone. For example, we have assumed that the residual deposition stresses are fully relaxed before crystallization, and that pre-crystallization structural relaxation does not significantly contribute to the observed stress changes. It should also be noted that the densities of our vapor-deposited films may be systematically lower than those of glasses formed by liquid quenching, owing to the high effective quench rate of vapor deposition. Although these effects could possibly change the calculated absolute magnitudes of the volume changes, the general trend shown in Fig. 3A (three peaks in the density change) is likely to remain unchanged.

The critical thickness for glass formation determined from the wedge-casting experiments (Fig. 3B) follows the trend seen for the density change, with a smaller density change corresponding to larger critical thicknesses (and therefore to easier glass formation). The three maxima of  $1.14 \pm 0.04$  mm at  $\text{Cu}_{50}\text{Zr}_{50}$ ,  $1.02 \pm 0.04$  mm at  $\text{Cu}_{56}\text{Zr}_{44}$ , and  $1.14 \pm 0.04$  mm at  $\text{Cu}_{64}\text{Zr}_{36}$  match the minima in the density change. These thicknesses match previously reported values (19–21).

The quench rate from a liquid that is required to produce a glass rather than a crystalline solid is a complex function of the interplay between kinetic constraints and the thermodynamic quantities that drive crystallization. The ease of glass formation is often found to correlate with small thermodynamic driving forces for crystallization (26), kinetic constraints on crystal nucleation and/or growth (27, 28), and high viscosity

in the undercooled liquid regime (26, 29). Quite a number of parameters based on these considerations have been proposed to evaluate the glass-forming ability of metallic alloys. However, none of the parameters can be used to provide a complete explanation for all three of the peaks in the critical thickness shown in Fig. 3B. For example, Turnbull's widely used criterion that the ease of glass formation correlates with a high reduced glass transition temperature  $T_{rg}$  ( $= T_g/T_l$ , where  $T_g$  is the glass transition temperature and  $T_l$  is the liquidus temperature) (27), can only be correlated with the peak corresponding to the eutectic composition  $\text{Cu}_{56}\text{Zr}_{44}$ . On the other hand, if we rely solely on the thermodynamic driving force for crystallization as an indicator, the peak at  $\text{Cu}_{50}\text{Zr}_{50}$  would not be expected, because intermetallic crystalline compound formation at  $\text{Cu}_{50}\text{Zr}_{50}$  should be much more energetically favored over glass formation as compared to adjacent compositions. The one-to-one match between the minima in the density change and the peaks of the critical thickness in Fig. 3 indicates that a small density change upon crystallization is a more fundamental factor in determining the ease of glass formation.

As previously reported by Mukherjee *et al.* (3), a liquid with a high density, as compared to its crystalline counterpart, has a lower content of free volume and a higher viscosity at its melting temperature. The volume change upon crystallization was correlated with the viscosity in accordance with the Cohen-Grest free volume theory (6–8). This would then result in a larger critical thickness measured in wedge-casting

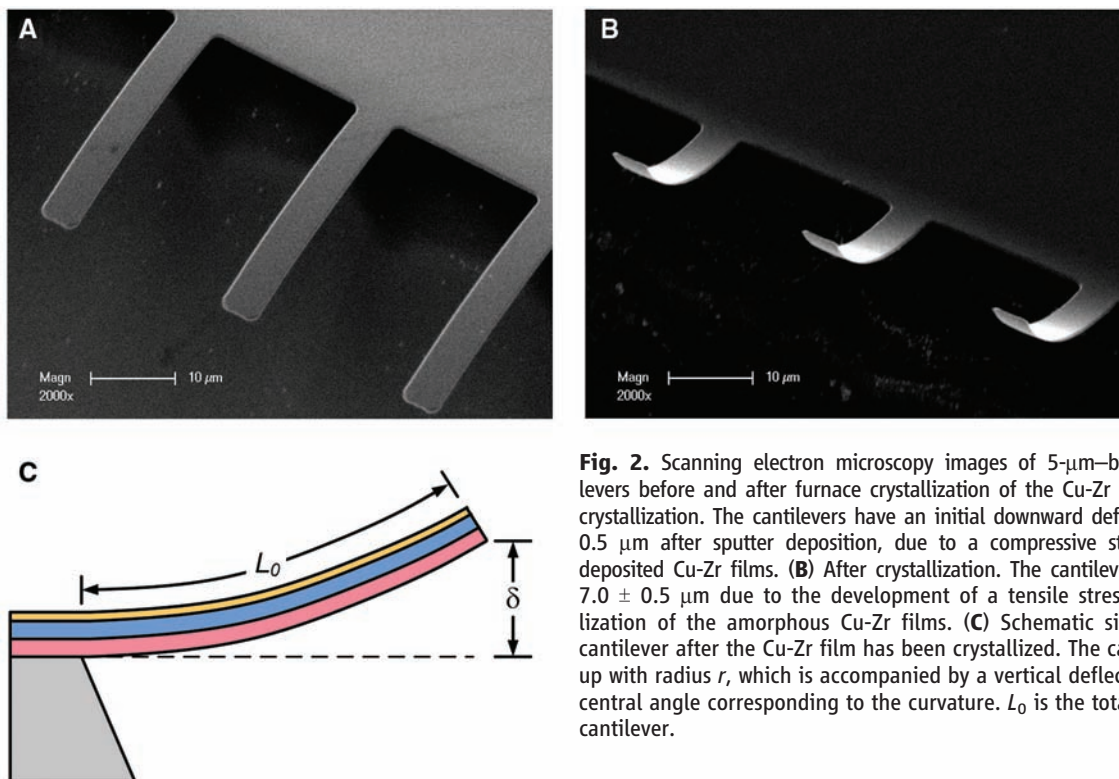


**Fig. 2.** Scanning electron microscopy images of 5- $\mu\text{m}$ -by-30- $\mu\text{m}$  cantilevers before and after furnace crystallization of the Cu-Zr film. **(A)** Before crystallization. The cantilevers have an initial downward deflection of  $3.0 \pm 0.5$   $\mu\text{m}$  after sputter deposition, due to a compressive stress in the as-deposited Cu-Zr films. **(B)** After crystallization. The cantilevers curve up by  $7.0 \pm 0.5$   $\mu\text{m}$  due to the development of a tensile stress upon crystallization of the amorphous Cu-Zr films. **(C)** Schematic side view of the cantilever after the Cu-Zr film has been crystallized. The cantilever curves up with radius  $r$ , which is accompanied by a vertical deflection  $\delta$ .  $\alpha$  is the central angle corresponding to the curvature.  $L_0$  is the total length of the cantilever.

experiments. The correlation between the density change and the critical thickness shown in Fig. 3 is consistent with this argument, although no direct measurements of viscosity have been made in this study.

Figure 4 shows the density of the amorphous phase ( $\rho_a$ ) as a function of alloying composition,

as obtained by subtracting the measured density change upon crystallization from the density of the equilibrium crystalline state. Also shown are previously measured densities for a few compositions of Cu-Zr metallic glasses taken from (25, 30–32).

Consistent with the trend shown in Fig. 3, there are three peaks in  $\rho_a$  at the compositions

corresponding to density-change minima. Although their magnitudes relative to the density baseline are only on the order of 1% higher, their correlation with glass-forming ability is established, suggesting a strong effect of density maxima. A successful structural model of metallic glasses must account for the three distinct compositions with correlated maxima in the density of the amorphous phase and minima in the cooling rate required to form a glass. Unfortunately, it seems that none of the existing models have these capabilities. For example, the dense-random-packing model leads to the expectation of only one peak, at  $\text{Cu}_{65}\text{Zr}_{35}$  (33), whereas the efficient-cluster-packing model (12) predicts only two densely packed structures at  $\text{Cu}_{18.0}\text{Zr}_{82.0}$  (for Cu-centered cluster packing) and  $\text{Cu}_{90.9}\text{Zr}_{9.1}$  (for Zr-centered cluster packing), respectively. The Ma model (13) applies to alloys of low solute contents and is therefore not applicable to the  $\text{Cu}_{50}\text{Zr}_{50}$  case, and the Egami-Waseda topological model (34) only gives the minimum solute concentration needed for glass formation, which is 10.8 atomic % for Zr and 20.8 atomic % for Cu in the Cu-Zr system. Therefore, although all of these models are fundamentally based on the dense packing concept, they cannot fully explain the correlation between the density and structure of metallic glasses and the ease of glass formation. Owing to the relatively small magnitudes of the density maxima, we speculate that they are related to a change in the short-range atomic order in the amorphous phase.

We have developed and demonstrated an effective and efficient combinatorial method for the investigation of the compositional dependence of the density change upon crystallization, over broad compositional ranges with high resolution. Using the Cu-Zr binary system, we have shown that there is a clear correlation between the density change and the glass-forming ability, which is consistent with models that suggest that glass formation correlates with reduced diffusivity in the glassy state. Moreover, the three density peaks for the amorphous phase suggested by this work not only correlate with the ease of glass formation but are also unexpectedly and unexplainably sharp. Our results provide evidence for the dense packing phenomenon in metallic glasses and provide new data to prompt improved modeling of their structures. The experimental methodology adopted in this work can be applied to other binary systems and more complex multicomponent systems, providing a new tool for broad investigations of the properties of glass-forming alloy systems, as well as for the search for new glass-forming alloys.

**Fig. 3.** Density change upon crystallization ( $(\rho_c - \rho_a)/\rho_a$ ) (A), and the critical thickness for glass formation (B) versus Zr content (atomic %). The density change axis is inverted, to make the two plots more directly comparable. The error of the composition measurement (A) is estimated to be  $\pm 1.0$  atomic %. In the wedge-casting experiments (B), the error of the critical thickness measurement is  $\pm 0.04$  mm, and the variation of the composition can be controlled within  $\pm 0.05$  atomic %

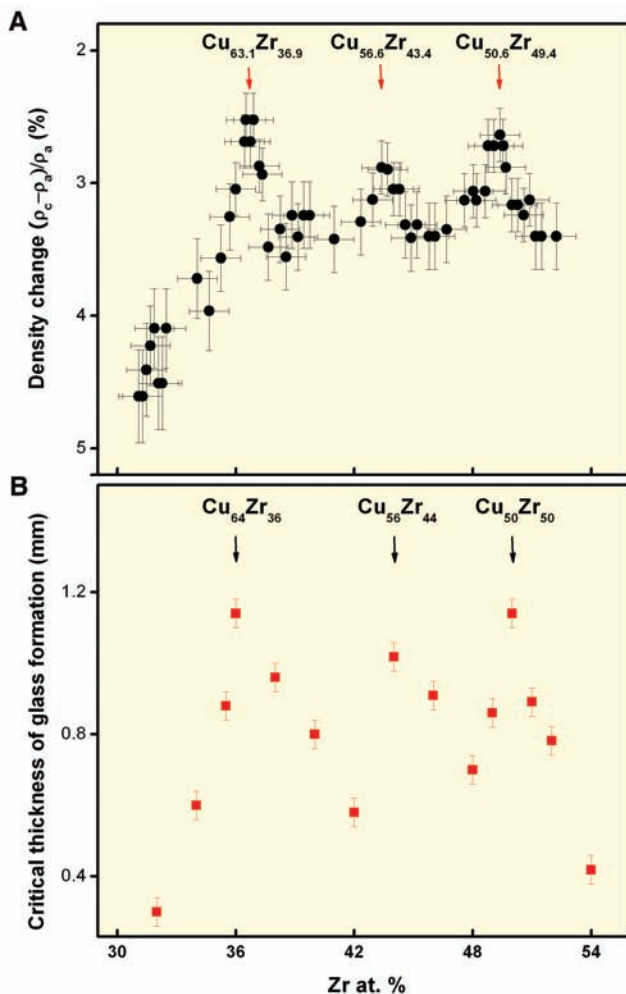
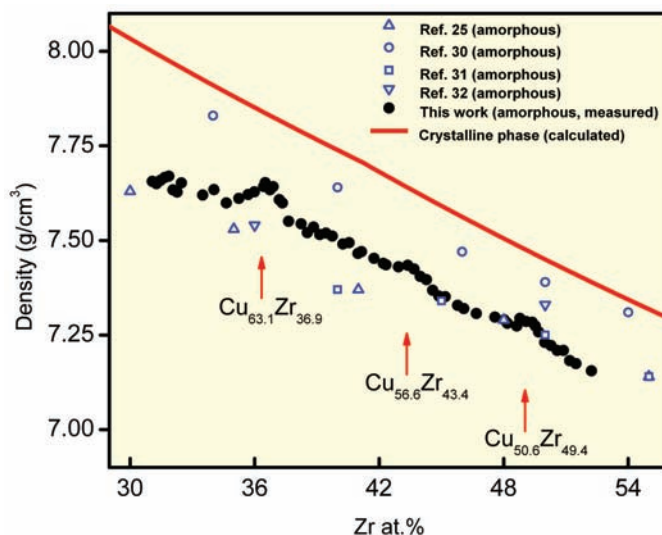


**Fig. 4.** Density plot for different compositions in the binary Cu-Zr system. The density of the crystalline phase (estimated from the equilibrium phase diagram using the lever rule), the density of the amorphous phase (estimated from the density change upon crystallization in the present study and the density of the crystalline phase), and density data for Cu-Zr metallic glasses reported in the literature (25, 30–32) are shown.



#### References and Notes

1. A. Inoue, N. Nishiyama, *Mater. Res. Bull.* **32**, 651 (2007).
2. A. L. Greer, E. Ma, *Mater. Res. Bull.* **32**, 611 (2007).
3. S. Mukherjee, J. Schroers, Z. Zhou, W. L. Johnson, W.-K. Rhim, *Acta Mater.* **52**, 3689 (2004).
4. A. R. Yavari, *Phys. Lett.* **95A**, 165 (1983).
5. A. R. Yavari, A. Inoue, *Mater. Res. Soc. Symp. Proc.* **554**, 21 (1999).

6. D. Turnbull, M. H. Cohen, *J. Chem. Phys.* **34**, 120 (1961).
7. D. Turnbull, M. H. Cohen, *J. Chem. Phys.* **52**, 3038 (1970).
8. M. H. Cohen, G. S. Grest, *Phys. Rev. B* **20**, 1077 (1979).
9. D. B. Miracle, W. S. Sanders, O. N. Senkov, *Philos. Mag.* **83**, 2409 (2003).
10. T. Egami, *J. Alloy. Comp.* **434-435**, 110 (2007).
11. F. Faupel *et al.*, *Rev. Mod. Phys.* **75**, 237 (2003).
12. D. B. Miracle, *Acta Mater.* **54**, 4317 (2006).
13. H. W. Sheng, W. K. Luo, F. M. Alamgir, J. M. Bai, E. Ma, *Nature* **439**, 419 (2006).
14. X. Hu, S. C. Ng, Y. P. Feng, Y. Li, *Phys. Rev. B* **64**, 172201 (2001).
15. A. Inoue, T. Negishi, H. M. Kimura, T. Zhang, A. R. Yavari, *Mater. Trans. Jpn. Inst. Metals* **39**, 318 (1998).
16. T. D. Shen, Y. He, R. B. Schwarz, *J. Mater. Res.* **14**, 2107 (1999).
17. J. A. Kalb *et al.*, *J. Microelectromech. Syst.* **17**, 1094 (2008).
18. D. Xu, B. Lohwongwatana, G. Duan, W. L. Johnson, C. Garland, *Acta Mater.* **52**, 2621 (2004).
19. M. B. Tang, D. Q. Zhao, M. X. Pan, W. H. Wang, *Chin. Phys. Lett.* **21**, 901 (2004).
20. D. Wang *et al.*, *Appl. Phys. Lett.* **84**, 4029 (2004).
21. A. Inoue, W. Zhang, *Mater. Trans. Jpn. Inst. Metals* **45**, 584 (2004).
22. N. Mattern *et al.*, *J. Non-Cryst. Solids* **354**, 1054 (2008).
23. J. A. Floro *et al.*, *J. Appl. Phys.* **89**, 4886 (2001).
24. S. G. Mayr, K. Samwer, *Phys. Rev. Lett.* **87**, 036105 (2001).
25. Z. Altounian, G. H. Tu, J. O. Strom-Olsen, *J. Appl. Phys.* **53**, 4755 (1982).
26. B. Busch, J. Schroers, W. H. Wang, *Mater. Res. Bull.* **32**, 620 (2007).
27. D. Turnbull, *Contemp. Phys.* **10**, 473 (1969).
28. D. Ma, H. Tan, D. Wang, Y. Li, E. Ma, *Appl. Phys. Lett.* **86**, 191906 (2005).
29. S. Mukherjee, J. Schroers, W. K. Rhim, W. L. Johnson, *Phys. Rev. Lett.* **94**, 245501 (2005).
30. Y. J. Calvayrac, J. P. Chevalier, M. Harmelin, A. Quivy, J. Bigot, *Philos. Mag. B* **48**, 323 (1983).
31. Z. Altounian, J. O. Strom-Olsen, *Phys. Rev. B* **27**, 4149 (1983).
32. L. A. Davis, C.-P. Chou, L. E. Tanner, R. Ray, *Scripta Met.* **10**, 937 (1976).
33. J. C. Lee *et al.*, *J. Mater. Res.* **22**, 3087 (2007).
34. T. Egami, Y. Waseda, *J. Non-Cryst. Solids* **64**, 113 (1984).
35. Q.G. acknowledges the Singapore-MIT Alliance for a graduate student fellowship and J.A.K. acknowledges partial financial support from the Alexander-von-Humboldt Foundation. We thank C. Sow for help with optical microscopy and G. Chen for help with the furnace annealing experiments.

#### Supporting Online Material

www.sciencemag.org/cgi/content/full/322/5909/1816/DC1

Materials and Methods

Figs. S1 to S3

References

10 July 2008; accepted 18 November 2008

10.1126/science.1163062

# Stable Prenucleation Calcium Carbonate Clusters

Denis Gebauer, Antje Völkel, Helmut Cölfen\*

Calcium carbonate forms scales, geological deposits, biominerals, and ocean sediments. Huge amounts of carbon dioxide are retained as carbonate ions, and calcium ions represent a major contribution to water hardness. Despite its relevance, little is known about the precipitation mechanism of calcium carbonate, and specified complex crystal structures challenge the classical view on nucleation considering the formation of metastable ion clusters. We demonstrate that dissolved calcium carbonate in fact contains stable prenucleation ion clusters forming even in undersaturated solution. The cluster formation can be characterized by means of equilibrium thermodynamics, applying a multiple-binding model, which allows for structural preformation. Stable clusters are the relevant species in calcium carbonate nucleation. Such mechanisms may also be important for the crystallization of other minerals.

Calcium carbonate has great scientific relevance in biomineralization and geosciences, forming enormous scales of biological (reefs and ocean sediments) and geological origin, which bind a huge amount of CO<sub>2</sub> and affect the chemistry of ocean water (1) and, with it, Earth's atmosphere and climate. Scale formation (incrustation) also affects daily life, industry, and technology and can require the addition of scale inhibitors to laundry detergents and household cleaners and in many industrial applications. Scale formation also lowers the efficiency of heating and cooling devices and can result in machine damage. CaCO<sub>3</sub> provides a model system for nucleation and crystallization analysis of minerals for classical (2) and non-classical crystallization (3) and has been studied for more than a century. Nevertheless, little is known about the very early stages of its crystallization, that is, the prenucleation stage. Amorphous calcium carbonate (ACC) is identified as a postnucleation-stage precursor phase in calcium

carbonate mineralization (4, 5), in bio- (6) and biomimetic mineralization (7), and liquid precursors have been identified in some cases (8). There is growing evidence that different species of ACC exist, that is, where the amorphous phase shows a specific short-range order that corresponds to the long-range order of the particular crystalline polymorph (9–11). Besides stable biogenic species, ACC occurs as a transient precursor phase in biomineralization. Precursor species that form still earlier than ACC or liquid precursors—that is, directly after ion contact and before nucleation occurs—have been postulated (12) and suggested through modeling approaches (13).

In the classical picture, nucleation is considered to take place in a solution of ions that has become supersaturated, leading to the nucleation of the solid phase by stochastic solute clustering, and the earliest crystal precursor is considered to be a cluster of critical size (14, 15). Because of the stochastic formation mechanism, such metastable clusters are a rare species. In contrast, there is increasing evidence that small polymeric species and stable clusters play a dominant role in the prenucleation stage of biomineralization and the formation of organic nanoparticles (16, 17).

Such soluble species have been reported for the polycondensation of silicic acid (18), precipitation of aluminum oxyhydroxide (19), and aqueous solutions of hydrated ions of the transition metals iron, chromium, uranium, molybdenum, and tungsten (20). In the above examples, the prenucleation cluster formation is a polymerization-like event, because the chemical bonds formed are mostly covalent (silica) to partly ionic (transition metals). For nonpolymerizing ionic crystals, solute clustering has been reported only for highly soluble compounds such as citric acid, urea, sodium nitrate, and potassium sulfate (21) and in supersaturated solutions (22). Cluster formation for low concentrations, that is, undersaturated and slightly supersaturated ionic solutions, has not been reported, and even advanced data analysis like induction time statistics do not allow for the accurate observation of all subcritical species present in a dilute system (23, 24).

Our experiments are based on the measurement of Ca<sup>2+</sup> concentrations at constant pH values, facilitating a quantitative determination of all species present at the different stages of crystallization while the supersaturation slowly evolves. This is achieved by slow addition of dilute calcium chloride solution into dilute carbonate buffer to induce supersaturation, causing nucleation and precipitation of calcium carbonate. The experimental set-up is described in detail in supporting online material (SOM) section 1 (fig. S1). The increase in calcium ions is shown for a single experiment at pH = 9.25 (Fig. 1A). The red line reflects the amount of calcium ions added. However, the amount of free calcium ions detected by the calcium ion selective electrode (black line) increases considerably slower straight from the beginning of the experiment; that is, a distinct part of free calcium ions disappears due to binding. The prenucleation-stage time development is linear, indicating that the calcium binding behavior in under- and supersaturated stages of the prenucleation stage is equal. Once a critical point is reached, nucleation occurs and the amount of free calcium ions drops

Max Planck Institute of Colloids and Interfaces, Research Campus Golm, Am Mühlenberg 1, D-14424 Potsdam, Germany.

\*To whom correspondence should be addressed. E-mail: coelfen@mpikg.mpg.de